JOURNAL OF GUIDANCE, CONTROL, AND DYNAMICS
Vol. 20, No. 1, January–February 1997

Attitude Estimation Algorithms for Spinning Satellites Using Global Positioning System Phase Data

Penina Axelrad* and Charles P. Behre†
University of Colorado, Boulder, Colorado 80309

Several Global Positioning System (GPS) based attitude determination algorithms for spinning satellites are presented. Spin rate and nutation frequencies are identified by fast Fourier transform and autoregressive model methods. Attitude angles are estimated using a simple cross-product method and a batch processing algorithm. These techniques all use the GPS antenna displacement vector as the basic observable. Performance of the proposed methods is presented using both computer simulations and ground-based experimental data. Accuracies of better than 0.25 deg in attitude and 0.01 rpm in frequency are demonstrated.

Nomenclature

${}^{H}C^{B}$	= rotation matrix from B to H frame
${}^{I}C^{H}$	= rotation matrix from H to I frame
e	= subscript denoting experimental motion
$\hat{\boldsymbol{e}}$	= unit vector pointing from observer to Global Positioning System (GPS) satellite
$\hat{\boldsymbol{H}}$	= angular momentum unit vector
I_s	= spin axis moment of inertia
I_t	= transverse moment of inertia
k	= measurement time differencing interval
N	= number of measurements
$\boldsymbol{r}$	= slave antenna position vector relative to spacecraft center
$\boldsymbol{r}^{A}$	= vector expressed in A frame
r_o	= magnitude of $\boldsymbol{r}$
s	= subscript denoting simulated motion
α, β, γ	= rotation angles for ground tests
$\Delta\varphi$	= antenna phase difference measurement
$\boldsymbol{\delta r}$	= antenna displacement vector
$\delta\Delta\varphi$	= time-differenced $\Delta\varphi$ measurements
η, σ	= rotation angles from H to I frame
Θ	= antenna angular displacement
θ	= nutation angle
λ	= argument for equation for α
ν	= GPS receiver noise
ϕ	= antenna phase about angular momentum axis
ψ	= antenna phase about z body axis
ω	= inertial spin rate about the instantaneous rotation axis
ω_l	= inertial nutation rate
ω_p	= body nutation rate
ω_α	= tipping rate

I. Introduction

LOW-COST satellite missions such as the Student Nitric Oxide Explorer[1] are designed to spin about the spacecraft major axis for both attitude stabilization and instrument scanning of the Earth. This type of spacecraft typically does not have very stringent attitude control requirements; however, both position and attitude knowledge to better than 1 km and 1 deg, respectively, are needed for postmission analysis of the scientific data. Global Positioning System (GPS) has the potential to provide this information cost effectively and at low weight and power.

Received March 13, 1996; revision received Aug. 3, 1996; accepted for publication Aug. 8, 1996.

*Assistant Professor, Colorado Center for Astrodynamics Research, Campus Box 431. Member AIAA.

†Research Assistant, Colorado Center for Astrodynamics Research, Campus Box 431. Student Member AIAA.

The use of GPS for spacecraft attitude determination onboard an Earth-pointing spacecraft already has been demonstrated on the U.S. Air Force RADCAL (Radar Calibration) satellite[2,3] and the Crista Spas missions.[4,5] In general, a minimum of three antennas is required for full attitude estimation. Phase difference measurements between antennas from two or more satellites form the basis for the attitude estimation algorithms.

The application of GPS specifically to spinning satellites was suggested by Martin–Neira and Lucas[6] in 1992. They described a fast Fourier transform (FFT)-based method for using a single GPS antenna baseline to determine spacecraft spin and nutation rates as well as nutation angles and orientation of the angular momentum vector. Their approach uses triple-differenced phase measurements as the basic observable.

Attitude determination of a spinning vehicle with GPS is particularly attractive because of the inherent baseline motion. This regular motion permits direct three-axis attitude estimation with a single baseline, i.e., two antennas or in some cases even a single GPS antenna. This may result in a reduction in onboard hardware or improved redundancy with existing hardware. Furthermore, the baseline motion permits highly accurate solutions to be obtained from time-differenced observations, thus eliminating the need for ambiguity resolution and minimizing the effect of cycle slips.

This paper discusses and compares several algorithms for estimation of the spinning spacecraft angular rates and orientation of the angular momentum vector based on GPS phase data. Analysis is conducted on data from a computer simulation and from a ground experiment. We begin with a discussion of the GPS observables and of the spinning satellite motion. This is followed by a description of ground-based experiments. The next section presents three techniques for determining the spacecraft spin rates. The first is a simple averaging method. The other two are frequency domain approaches: the FFT method, used by Martin-Neira and Lucas,[6] and a superior autoregressive (AR) method. Finally, two methods for determining the orientation of the spacecraft angular momentum vector are discussed. One uses an averaging technique. The other uses a batch processor.

II. Displacement Vectors

Time-differenced GPS phase observations have been used in surveying to establish an initial estimate for long antenna baselines[7] and in attitude determination as a means for initial ambiguity resolution.[8] In general, they do not produce high-accuracy estimates because the measurement noise is higher and the geometry is weaker than a single-difference (between antennas) or double-difference (between antennas and satellites) observable. The latter problem is not the case for a spinning satellite, where the rapid antenna motion produces a strong geometry for time-differenced observations. The time-difference observations are used to solve for what we call antenna displacement vectors, which form the basis for the attitude solution methods described subsequently.

Note that the receiver is assumed to be operating in a steady-state condition, that is, it has already acquired at least four satellites and is computing position solutions in real time. The acquisition process typically takes up to 30 s for a receiver that has been initialized with an a priori estimate of the orbit, GPS ephemeris, and time, and up to 30 min for a receiver in cold start. In addition, it is assumed that the receiver generates phase difference observations $\Delta\varphi$ between two antennas and computes appropriate line-of-sight vectors $\hat{\boldsymbol{e}}$ to the GPS satellites, based on its current navigation solution.

The basic equation for the $\Delta\varphi$ measurement for one baseline and from one satellite is

$$\Delta\varphi = \hat{\boldsymbol{e}} \cdot \boldsymbol{r} - b + v \tag{1}$$

where b is a bias due to an integer ambiguity and a line or clock bias between antennas. By differencing two $\Delta\phi$ measurements made at times t_i and t_{i+k}, assuming no cycle slips, and approximating the line-of-sight vector as constant over this interval, an equation involving the antenna displacement vector $\boldsymbol{\delta r}$ can be formed as

$$\delta\Delta\varphi(t_i) \equiv \Delta\varphi(t_{i+k}) - \Delta\varphi(t_i) = \hat{\boldsymbol{e}}(t_i) \cdot \boldsymbol{\delta r}(t_i) + (v_{i+k} - v_i) \tag{2}$$

and k is a constant differencing interval. Cycle slips and temporary blockages or shadowing of the antennas will corrupt only a single $\delta\Delta\varphi$ measurement, thus making this a relatively robust observable.

To solve Eq. (2) for $\boldsymbol{\delta r}$, measurements from at least three GPS satellites must be available. If we assume that the noise is uncorrelated, unbiased, and equivariant, then the least-squares solution is

$$\boldsymbol{\delta r}(t_i) = (G^T G)^{-1} G^T \begin{bmatrix} \delta\Delta\varphi^1(t_i) \\ \delta\Delta\varphi^2(t_i) \\ \vdots \\ \delta\Delta\varphi^M(t_i) \end{bmatrix} \tag{3}$$

where

$$G = [\hat{\boldsymbol{e}}^1 \quad \hat{\boldsymbol{e}}^2 \quad \ldots \quad \hat{\boldsymbol{e}}^M]^T \tag{4}$$

the superscript refers to each satellite, and M is the number of satellites.

III. Spinning-Satellite Model

The nutation angle and various angular rates, defined in the nomenclature section, are illustrated in Fig. 1. For simplicity, the vehicle is assumed to be axisymmetric about the z^B axis. The master antenna is located at the center with the master–slave baseline perpendicular to the axis of symmetry. The body x^B axis is defined by the position of the slave antenna. The relationships between ω, ω_p, ω_l, θ, and the inertias are[9]

$$\omega_p = \frac{I_t - I_s}{I_s}\omega_l \cos\theta \tag{5}$$

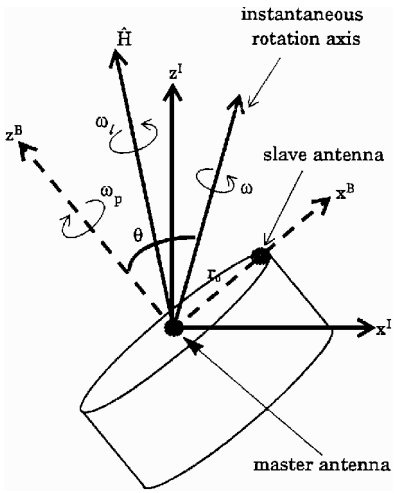

Fig. 1 Kinematic model.

and

$$\omega^2 = \omega_p^2 + \omega_l^2 + 2\omega_p\omega_l \cos\theta \tag{6}$$

The body frame is fixed to the rotating satellite and is denoted by superscript B. The angular momentum frame, denoted by the superscript H, is defined with the z axis along the spacecraft angular momentum vector. The inertial frame is designated by the superscript I. The angular momentum vector unit vector $\hat{\boldsymbol{H}}_s$ in the inertial frame is

$$\hat{\boldsymbol{H}}_s^I = [h_x \quad h_y \quad h_z]^T \tag{7}$$

A. Antenna Motion

In the absence of external torques, a GPS antenna on the rim of a spinning satellite will move according to the kinematic model described in Eqs. (5) and (6). In the body fixed system, the antenna position remains constant. The position of the antenna with respect to the center of the spacecraft in the inertial system can be computed from the product of two separate rotation matrices given by

$$\boldsymbol{r}^I = {}^I C_s^H \, {}^H C_s^B \boldsymbol{r}^B \tag{8}$$

where

$$\boldsymbol{r}^B = [r_o \quad 0 \quad 0]^T \tag{9}$$

is the position of the antenna in the body frame. The first rotation, ${}^H C_s^B$, takes $\boldsymbol{r}$ from the body to the angular momentum frame. The angles ψ and ϕ are defined as functions of the satellite rotation rates as follows:

$$\psi = \omega_p t + \psi_o, \qquad \phi = \omega_l t + \phi_o \tag{10}$$

Then ${}^H C_s^B$ can be expressed as

$${}^H C_s^B = \begin{bmatrix} c\psi c\phi - c\theta s\psi s\phi & -s\psi c\phi - c\theta c\psi s\phi & s\theta s\phi \\ c\psi s\phi + c\theta s\psi c\phi & -s\psi s\phi - c\theta c\psi c\phi & s\theta c\phi \\ s\theta s\psi & s\theta c\psi & c\theta \end{bmatrix} \tag{11}$$

The matrix ${}^I C_s^H$ rotates a vector from the angular momentum system to the inertial system. It is defined by the two angles η and σ, which are determined from the components of the angular momentum unit vector by

$$\eta = \cos^{-1}\left(\frac{h_x}{\sqrt{h_x^2 + h_y^2}}\right) \tag{12}$$

and

$$\sigma = \cos^{-1}(h_z) \tag{13}$$

This matrix is

$${}^I C_s^H = \begin{bmatrix} c\eta c\sigma & -s\sigma & c\eta s\sigma \\ s\eta c\sigma & c\eta & s\eta s\sigma \\ -s\sigma & 0 & c\sigma \end{bmatrix} \tag{14}$$

If Eq. (8) is differenced in time, an expression relating the antenna displacement vectors to the satellite kinematics can be formulated. For a constant orientation of a satellite angular momentum vector, this relationship at time t_i is

$$\boldsymbol{\delta r}^I(t_i) = {}^I C_s^H \left[{}^H C_s^B(t_{i+k}) - {}^H C_s^B(t_i) \right] \begin{bmatrix} r_o \\ 0 \\ 0 \end{bmatrix} \tag{15}$$

The displacement vectors in the local frame are computed from the GPS phase differences by Eq. (3). Equation (15) describes how these components are related to the spacecraft attitude.

The frequencies observed in $\boldsymbol{\delta r}^I$ are due to the products of the sines and cosines in Eq. (11). The three frequencies are $\omega_l \pm \omega_p$ and ω_p.

B. Computer Simulation

A computer program was constructed to simulate the motion of a spinning satellite in low Earth orbit. Line-of-sight measurements

were generated from a simulated constellation of 24 GPS satellites using a typical set of orbital elements and taking into account satellite visibility limitations. Perfect phase difference values were formed from the line-of-sight and known antenna baseline vectors. Simulated $\Delta\varphi$ measurements were constructed by adding zero-mean Gaussian noise with a standard deviation of 5 mm. Displacement vectors were computed from the noisy $\Delta\varphi$ values. Measurements were recorded at 2 Hz for 12 min. The spin rate was 5 rpm, and the nutation angle was 5 deg.

IV. Ground Experiment

To validate the results of the computer simulation, a series of ground tests were conducted. Data were taken from a GPS receiver mounted on a spin table located at a Naval Research Laboratory test facility.

A. Experimental Apparatus

The complete test apparatus consists of two pieces of equipment with a combined total of three rotational axes as diagrammed in Fig. 2. A photograph of the actual setup is shown in Fig. 3. The TRT-7 two-axis tilter is mounted on a support base. In the local level coordinate frame, the first axis is oriented along an east–west direction. The second axis is aligned perpendicular to the first and rotates around it. When the first rotation angle is zero, the second axis lies in the north–south direction. The maximum tilt angle about both axes is approximately ±45 deg. The second piece of equipment is the BDS-5 spinner. It provides a constant angular rate about a third axis. This axis rotates according to the tilt angles of the TRT-7. It is mounted so that, when the first two rotation angles are zero, its orientation is in the up–down direction. The GPS antennas are mounted on the top plane of the satellite structure perpendicular to this axis.

B. Experimental Motion

The matrix ${}^{H}C_{s}^{B}$, derived in Eq. (11), is a 3-1-3 sequence of rotations computed from the Euler angles ψ, ϕ, and θ. The satellite structure in the experimental setup has to be moved according to the rotations defined by the TRT-7 and the BDS-5. For this case, the body frame is defined by the symmetry axis of the structure and the position of one of the GPS antennas, as shown in Fig. 2. In the body frame the position of the GPS antenna is always on the x^B axis. The local system is defined by the orientation of the TRT-7's tilt axis when the plane of the structure is level to the ground. Although there is no true angular momentum axis, an equivalent frame to the angular momentum frame is defined by the plane of the satellite structure when there is only pure spin. This is referred to as the H frame.

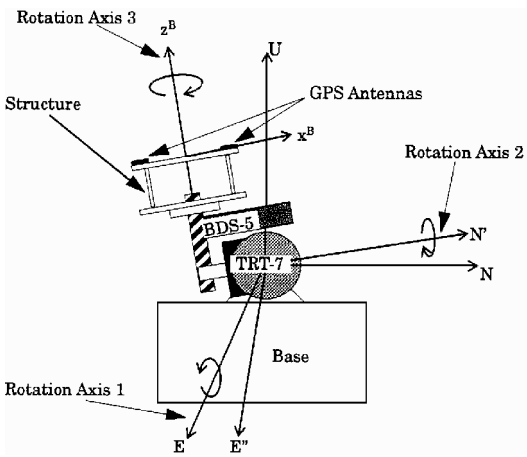

Fig. 2 Equipment diagram.

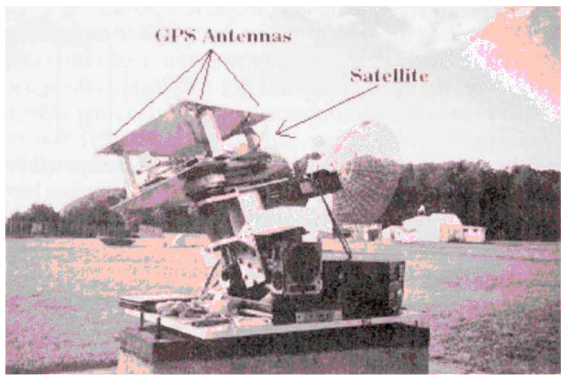

Fig. 3 Experimental setup.

If the east direction is called the 1 axis, the north direction the 2 axis, and the up direction the 3 axis, then the series of rotations used to move the GPS antenna is a 1-2-3 sequence. If we define the three rotation angles as β, α, and γ, respectively, then the total rotation matrix is

$$ {}^{B}C_{e}^{H}(\beta,\alpha,\gamma) = R_3(\gamma)R_2(\alpha)R_1(\beta) \tag{16} $$

To simulate the correct movement of a GPS antenna on a spinning satellite governed by Eq. (11), the angles β, α, and γ must be varied in time as a function of ψ, ϕ, and θ. These relations are computed by setting

$$ {}^{B}C_{e}^{H}(\beta,\alpha,\gamma) = {}^{B}C_{s}^{H}(\phi,\theta,\psi) \tag{17} $$

The resulting expressions for α, β, and γ are functions of the sums and products of the sinusoids of ϕ, θ, and ψ. These general equations are very involved; however, for small nutation angles, they may be approximated by

$$ \beta(t) \approx \theta \sin[\phi(t)] \tag{18} $$

$$ \alpha(t) \approx \theta \cos[\phi(t)] \tag{19} $$

and

$$ \gamma(t) \approx \phi(t) + \psi(t) \tag{20} $$

Because of limitations in the control and performance of the test equipment, two compromises are required. The first is to eliminate the motion of β due to Eq. (18). The second is to approximate the motion of α in Eq. (19) with a triangle wave. The equation for α is

$$ \alpha(t) \approx \theta(8/\pi^2)\left\{\sin[\lambda(t)] - \tfrac{1}{9}\sin[3\lambda(t)] + \tfrac{1}{25}\sin[5\lambda(t)] - \cdots\right\} \tag{21} $$

where

$$ \lambda(t) = \omega_\alpha t + \lambda_o \tag{22} $$

and

$$ \omega_\alpha = (2\theta/\pi)\omega_l \tag{23} $$

Combining the motion of α about the 2 axis and the motion of γ about the 3 axis yields the rotation matrix from the body system to the angular momentum system:

$$ {}^{H}C_{e}^{B} = \begin{bmatrix} c\gamma c\alpha & -s\gamma c\alpha & s\alpha \\ s\gamma & c\gamma & 0 \\ -c\gamma s\alpha & s\gamma s\alpha & c\alpha \end{bmatrix} \tag{24} $$

The resulting motion described by Eq. (24) and illustrated in Fig. 4 is a combination of spinning and tipping. The tipping is contained in a single plane centered on the $\hat{\boldsymbol{H}}_e$ axis. The orientation of $\hat{\boldsymbol{H}}_e$ is fixed and described by the two angles σ and η. The angle σ is about the 1 axis and the angle η is about the 2 axis. The corresponding rotation matrix from the angular momentum system to the inertial system is

$$ {}^{I}C_{e}^{H} = \begin{bmatrix} c\eta & 0 & s\eta \\ s\eta s\sigma & c\sigma & -c\eta s\sigma \\ -s\eta c\sigma & s\sigma & c\eta c\sigma \end{bmatrix} \tag{25} $$

The rotation matrices in Eqs. (24) and (25) are analogous to the matrices in Eqs. (11) and (14) for the true satellite rotations. One difference is that in the case of an actual spinning satellite, the spin axis rotates about the angular momentum axis, whereas for the experimental motion the spin axis tips about some central axis. Another difference is in the frequency modes of the ground experiments.

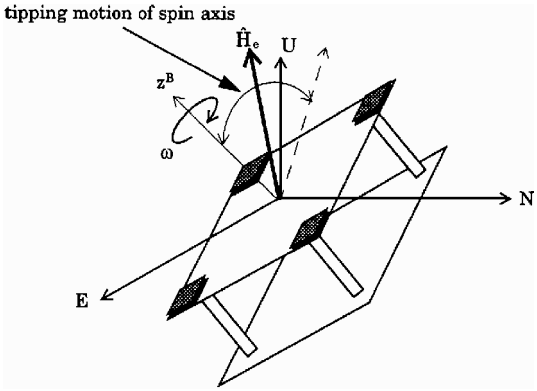

Fig. 4 Spinning and tipping motion.

C. Experimental Motion Frequencies

It was shown that the equations for satellite motion contain three frequencies derived from the two satellite rates of ω_p and ω_l. The frequencies contained in the experimental motion are similar. For this case the two principal rates are ω and ω_α and the observed frequencies are at ω and $\omega \pm k\omega_\alpha$, where k is any integer. As before, there is a frequency due to the rate about the spin axis and frequencies due to the combined rates of the spin axis about a fixed vector. Because $\alpha(t)$ is a triangle wave, it also contains odd harmonies of ω_α as opposed to just a single frequency. Thus cosine α contains even multiples and the sine α contains odd ones. A power spectral density (PSD) plot of the displacement vectors yields an infinite number of spikes corresponding to all possible values of k. However, only the first few multiples of ω_α have enough power to show above the noise floor.

The reference value for the ground test spin rate was 0.0850 Hz $\pm$ 7×10^{-5} Hz. The platform was leveled to within 1 deg and the initial alignment error was determined to be ± 0.01 deg.

D. GPS Receiver

The experiments were conducted using a Trimble Navigation TANS Vector Attitude Receiver.[10,11] This receiver has six parallel tracking channels that multiplex among four antennas to provide attitude estimates as well as navigation solutions. One antenna is designated as the master, and the other three are slaves. The receiver measures the relative carrier phase for each slave with respect to the master. For our experiments we collected these raw differential phase data at a rate of 2 Hz. Typical differential phase errors for the receiver are in the range of 2–5 mm 1-sigma, depending on the signal environment.[12]

The next sections describe various algorithms for attitude and frequency estimation.

V. Frequency Estimation Techniques

In this section, three frequency estimation techniques are examined. The first method is a time-domain technique, and the next two are frequency-domain methods.

A. Displacement-Vector-Magnitude Algorithm

The simplest approximation for the angular velocity ω given in Eq. (6) can be computed from the magnitude of $\boldsymbol{\delta r}$. Every two successive positions of a rotating antenna creates an angular displacement centered at the spin axis. This angle, shown in Fig. 5, can be computed by

$$\Theta = 2\sin^{-1}\left(\frac{\frac{1}{2}|\boldsymbol{\delta r}|}{r_o}\right) \tag{26}$$

where $r_o = |\boldsymbol{r}|$. If we define ω^* as the mean angular rate of Θ, then the magnitude of ω^* varies with ω_p, its minimum value is $[I_t/(I_t - I_s)]\omega_p$, and its maximum value is ω. For a nutation angle of zero, $\omega = \omega^*$. As a result, for small nutation angles, ω can be approximated by averaging the values of ω^* computed from the displacement vectors. Furthermore, if an accurate value of the satellite's inertia ratio is known, an estimate of ω_p and ω_l also can be found.

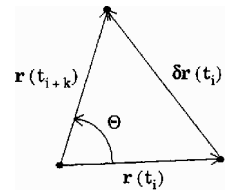

Fig. 5 Angular displacement.

B. FFT Algorithm

To determine the modal frequencies and modal amplitudes of a signal, the following steps are applied: Perform an FFT on the sampled signal data, compute the PSD of the transformed data, identify the peaks of the PSD, determine the frequency at which each peak occurs, and relate these frequencies back to a kinematic model.

If only the PSD values are used, then the frequencies are the most likely estimates of each signal mode. Ideally, they are the exact frequencies of the modes. However, the sampling properties of the signal can lead to errors.

The frequency resolution is equal to the sample frequency divided by the number of data points. Ideally, the signal should be sampled so that the modal frequencies are integer multiples of the frequency bin. In reality, however, the peaks of the PSD occur in the frequency bins that are closest to the correct modes. The signal power of each mode is spread over a range of frequency bins surrounding the correct frequency. To determine a better estimate, the frequency center of the bins can be computed by weighting them according to their power. However, the benefit of this approach may be limited by noise.

In the implementation of an FFT algorithm, there are no assumptions about the structure of the signal. In other words, the FFT can be applied to any type of signal. There are other frequency estimation methods that can take advantage of the knowledge of the signal's structure. The next section discusses one of these methods—the AR method.

C. AR Algorithm

In general, a discrete-time process can be approximated well by a time series or rational transfer function model.[13] In particular, a system of order $2p$ can be represented by the recursive difference relation

$$x[n] = -\sum_{k=1}^{2p} a[k]x[n-k] + u[n] \tag{27}$$

Taking the Z transform of Eq. (27) yields the transfer function

$$X(z)/U(z) = 1/P(z) \tag{28}$$

where

$$z = e^{\sigma + j\theta} \tag{29}$$

and

$$P(z) = 1 + \sum_{k=1}^{2p} a[k]z^{-k} \tag{30}$$

Given a sequence of sampled data $x[n]$, the coefficients $a[k]$ can be estimated using the modified covariance method.[7] The roots of $P(z)$ corresponding to sinusoids are described by

$$z_k^* = e^{\pm j\theta_k^*} \tag{31}$$

They occur in complex conjugate pairs and lie on the unit circle (i.e., $\sigma = 0$) at angles corresponding to the sinusoidal frequencies normalized by the sample frequency:

$$\theta_k^* = 2\pi \bar{f}_k, \qquad \bar{f}_k = f_k/f_s \tag{32}$$

Note that this technique directly estimates the modal frequencies and therefore does not provide estimates that are quantized by discrete frequency bins as does the FFT method.

Table 1 Performance of frequency methods on simulated data

	$N = 100$		$N = 200$		$N = 800$	
Method	ω_l, rad/s	ω_p, rad/s	ω_l, rad/s	ω_p, rad/s	ω_l, rad/s	ω_p, rad/s
True value	0.6789	−0.1561	0.6789	−0.1561	0.6789	−0.1561
AR	0.6760	−0.1530	0.6779	−0.1550	0.6794	−0.1565
FFT	No solution	No solution	0.6473	−0.1226	0.6795	−0.1562
Average ω^*	0.6780	−0.1565	0.6748	−0.1557	0.6759	−0.1560

Table 2 Performance of frequency methods on experimental data

	$N = 100$		$N = 200$		$N = 800$	
Method	ω, rad/s	ω_α, rad/s	ω, rad/s	ω_α, rad/s	ω, rad/s	ω_α, rad/s
Reference value	0.5349	——[a]	0.5349	——[a]	0.5349	——[a]
AR	0.5379	0.5807	0.5356	0.5959	0.5345	0.5973
FFT	No solution	No solution	0.5381	0.5947	0.5350	0.5971
Average ω^*	0.5337	——[b]	0.5350	——[b]	0.5358	——[b]

[a] There was no adequate reference value for ω_α. [b] The average ω^* method does not produce estimates for ω_α.

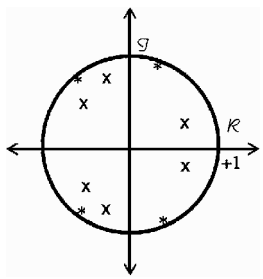

Fig. 6 Pole–frequency relationship for a noisy sampled signal; *, poles corresponding to signal; ×, poles corresponding to noise; model order = 10; and number of sinusoids = 2.

For the ideal case, where there is no noise, the signal is perfectly modeled by Eq. (30), with exactly p sinusoids, and each pole of Eq. (28) lies exactly on the unit circle at an angle of $2\pi\,\bar{f}_k$. For the more realistic case, a higher-order model than $2p$ is used to account for the noise in the signal. The poles corresponding to the signal modes lie closest to the unit circle, whereas the poles corresponding to the noise lie farther away. The angles of the signal mode poles are approximately equal to $2\pi\,\bar{f}_k$. This is illustrated in Fig. 6. As the model order is increased, there are more frequencies available for the noise. As a result, the poles for the signal modes get closer to the unit circle and the angles get closer to $2\pi\,\bar{f}_k$. The model order is limited by the number of samples, N. A maximum order of $N/2$ is recommended.[13] The model order used in this work is 70.

D. Frequency Estimation Results

Tables 1 and 2 compare the performance of the three frequency estimation techniques as a function of the data batch size. All data were sampled at 2 Hz. For the simulation, the nutation angle was 5 deg. For the experiment the maximum tip angle was 5.3 deg. The AR and average ω^* methods produced frequency errors under 0.01 rad/s after 30 s of data. The FFT methods could not resolve the frequencies with a data set this small and still showed large errors after 100 s. For large batch sizes, the errors were below 0.001 rad/s for both the AR and FFT techniques. Averaging ω^*, however, did not produce improvement with larger amounts of data. In the experiment the programmed value for ω_α was 0.628 rad/s. However, because of the limitations of the equipment noted earlier, we believe that this number was significantly in error. Judging by the consistency of the methods over various batch sizes and by the simulation results, our opinion is that the frequency estimation algorithms are much more accurate.

VI. Attitude Estimation Techniques

This section presents two methods for determining the orientation of the spacecraft angular momentum vector. The first technique uses the average of the displacement-vector cross products. The second uses a batch processor.

A. Cross-Product Algorithm

Ideally, a spinning satellite is rotating perfectly about its rotation axis (i.e., no nutation), which also will be its angular momentum axis. A GPS antenna located on one face of the satellite will rotate in a plane perpendicular to this axis. The displacement vector of the moving antenna will be in this plane. Taking the cross products of two of these vectors will yield a vector with the same orientation as the angular momentum axis. Because the GPS measurements are taken in the inertial frame, $\hat{\boldsymbol{H}}$ will be computed in the inertial frame. As a result, the components of $\hat{\boldsymbol{H}}$ define the orientation of the satellite spin axis in the inertial frame.

When nutation is introduced, the cross product of two successive displacement vectors is not the true orientation of $\hat{\boldsymbol{H}}$. However, as the satellite's instantaneous spin axis rotates about $\hat{\boldsymbol{H}}$, the average of all vectors formed from these cross products will tend toward the actual orientation of $\hat{\boldsymbol{H}}$. This is computed by

$$\hat{\boldsymbol{H}} = \frac{1}{N}\sum_{i=1}^{N} \frac{\boldsymbol{\delta r}(t_i) \times \boldsymbol{\delta r}(t_{i+k})}{|\boldsymbol{\delta r}(t_i) \times \boldsymbol{\delta r}(t_{i+k})|} \tag{33}$$

B. Spinning-Satellite Batch Processor

A batch-processing algorithm for estimation of the attitude was developed. The state comprises the nutation angle θ; the angular position of the antenna about the body z^B axis, ψ; the angular position about $\hat{\boldsymbol{H}}_s$, ϕ; and the two constant angles η and σ, which relate the inertial to the angular momentum frame. The resulting state vector is

$$\boldsymbol{X} = [\theta \quad \psi \quad \phi \quad \eta \quad \sigma]^T \tag{34}$$

For the torque-free case considered here, the state estimate is propagated between measurement epochs as follows:

$$\hat{\boldsymbol{X}}(t_{i+1}) = \hat{\boldsymbol{X}}(t_i) + \begin{bmatrix} 0 \\ \omega_p \delta t \\ \omega_l \delta t \\ 0 \\ 0 \end{bmatrix} \tag{35}$$

where

$$\delta t = t_{i+1} - t_i \tag{36}$$

The two frequencies must be determined by one of the previously described frequency estimation techniques.

The measurement model that relates the displacement vectors to the states is inherently nonlinear because the states are embedded in the elements of the attitude matrix. The nonlinear measurement equation is

$$\mathsf{h}(\boldsymbol{X}) = \frac{\boldsymbol{\delta r}^I(t_i)}{r_o} = {}^I C^H \left[{}^H C^B(t_{i+k}) - {}^H C^B(t_i) \right] \tag{37}$$

For the gain and covariance update calculations, the linearized measurement connection matrix is

$$\mathcal{H} \equiv \left.\frac{\delta \mathsf{h}}{\delta \boldsymbol{X}}\right|_{\hat{\boldsymbol{X}}_i} \tag{38}$$

Simulated data were generated using a nutation angle of 5 deg, an inertia ratio of 1.3, and a sample frequency of 2 Hz. The two driving frequencies, ω_p and ω_l, were -0.1561 and 0.6789 rad/s, respectively.

C. Ground-Experiment Batch Processor

The batch-processing algorithm for the experimental data is very similar to the one employed for the computer simulation. The estimated values are the angular position of the antenna about the body z^B axis, γ; the amplitude θ of the tipping motion; the argument for the equation for $\alpha(t)$, λ; and the two angles σ and η. The resulting state vector is

$$\boldsymbol{X} = [\gamma \quad \theta \quad \lambda \quad \eta \quad \sigma]^T \tag{39}$$

As described in Sec. IV, the induced motion was designed to simulate torque free satellite motion. As a result, the η and σ stay fixed. The magnitude and rate of the tipping motion remain constant. The position angles, γ and λ, change according to the two driving rates, ω and ω_α, respectively. The transition between measurement times is therefore

$$\hat{\boldsymbol{X}}(t_{i+1}) = \hat{\boldsymbol{X}}(t_i) + \begin{bmatrix} \omega\delta t \\ 0 \\ \omega_\alpha \delta t \\ 0 \\ 0 \end{bmatrix} \tag{40}$$

The driving frequencies are estimated using the frequency analysis techniques. The observation equations are the same as shown in Eqs. (37) and (38).

The phase difference $\Delta\varphi$ and line-of-sight measurements were collected at a sample rate of 2 Hz using a Trimble TANS Vector Receiver. The spin and tipping rates, ω and ω_α, were set at 0.535 and 0.597 rad/s, respectively. The tipping amplitude was 5.3 deg.

D. Estimation Results

Tables 3 and 4 show the performance of the attitude methods for various values of N for both the simulated and experimental cases. All data were taken at 2 Hz. For the simulation, the frequency was 5 rpm, and the nutation angle was 5 deg. For the experiment, the spin frequency was 5 rpm and the tipping rate was 2 deg/s. The estimation errors for η and σ are about the same when using either the cross-product or batch processor algorithms. When N is 400 or greater, the errors are under 0.1 deg. The batch processor allows for the estimation of additional parameters as well. For the largest batch sizes, the simulation nutation angle and the experimental tip angle are both determined to within 0.1 deg. Estimation of the phase angles is the least accurate. The simulation angles ψ and ϕ are determined to about 0.2 deg. However, the experimental angle γ is only estimated to within 2 deg.

Table 3 Performance of attitude methods on simulated data

Method	Angle	True value, deg	Estimated value, deg $N = 200$	$N = 400$	$N = 800$
$\boldsymbol{\delta r}$ Cross product	η	63.43	63.46	63.46	63.46
	σ	65.91	65.90	65.89	65.91
Batch processor	η	63.43	63.47	63.45	63.45
	σ	65.91	65.93	65.92	65.91
	θ	5.00	4.96	4.98	4.99
	ψ	90.00	91.82	90.34	89.83
	ϕ	90.00	88.23	89.59	90.18

Table 4 Performance of attitude methods on experimental data

Method	Angle	Reference value, deg	Estimated value, deg $N = 200$	$N = 400$	$N = 800$
$\boldsymbol{\delta r}$ Cross product	η	0.60	0.34	0.52	0.56
	σ	0.07	0.11	0.07	0.08
Batch processor	η	0.60	0.51	0.52	0.59
	σ	0.07	0.10	0.07	0.10
	θ	5.32	5.13	5.19	5.29
	γ	-47.38	-45.15	-44.74	-49.01
	α	1.01	0.78	0.82	1.11

VII. Conclusions

Several new algorithms for using GPS measurements to determine the attitude and angular rates of a spinning satellite are presented and demonstrated using both simulated orbital data and ground test data. The AR method is the best algorithm for determining spin rates. The $\boldsymbol{\delta r}$ cross-product method is the computationally simplest and fastest approach for estimating the angular momentum axis. The batch processor, however, produces estimates of more vehicle parameters. For batch sizes of 200 samples, corresponding to 100 s of data for a vehicle spinning at 5 rpm, spin rates are determined to within 0.01 rpm, spin-axis orientation is determined to within 0.25 deg, and phase to within 2 deg. Comparable performance could be expected for spacecraft in low Earth orbit, which would meet the requirements of many small satellite missions.

Acknowledgments

This research was sponsored by the Office of the Chief of Naval Research, U.S. Department of the Navy. The authors wish to thank Alan Hope of the Naval Research Laboratory and William Betts of the U.S. Air Force Academy for their help in conducting the experiments. In addition, we appreciate the very constructive suggestions of the associate editor and the anonymous reviewers.

References

[1]Barth, C. A., Solomon, S. C., Rusch, D. W., and Woods, T. N., "Student Nitric Oxide Explorer," Investigation and Technical Plan—Proposal to the Universities Space Research Association Student Explorer Demonstration Initiative, Lab. for Atmospheric and Space Physics, Univ. of Colorado, Boulder, CO, 1994.

[2]Lightsey, E. G., Cohen, C. E., Fees, W. A., and Parkinson, B. W., "Analysis for Spacecraft Attitude Measurements Using Onboard GPS," *Advances in the Astronautical Sciences*, Vol. 86, edited by R. Culp and R. Rausch, Univelt, San Diego, CA, 1994, pp. 521–532.

[3]Ward, L. M., and Axelrad, P., "Spacecraft Attitude Estimation Using GPS: Methodology and Results for RADCAL," *Proceedings of the ION National Technical Meeting* (Anaheim, CA), Inst. of Navigation, Alexandria, VA, 1995, pp. 813–825.

[4]Ward, L. M., "Spacecraft Attitude Estimation Using GPS: Methodology and Results," Ph.D. Dissertation, Dept. of Aerospace Engineering Sciences, Univ. of Colorado, Boulder, CO, Aug. 1996.

[5]Brock, J. K., Fuller, R., Kemper, B., Mleczko, D., Rodden, J., and Tadros, A., "GPS Attitude Determination and Navigation Flight Experiment," *Proceedings of ION GPS-95* (Palm Springs, CA), Inst. of Navigation, Alexandria, VA, 1995, pp. 545–554.

[6]Martin-Neira, M., and Lucas, R., "GPS Attitude Determination of Spin Stabilized Satellites," *Proceedings of ION GPS-92* (Albuquerque, NM), Inst. of Navigation, Alexandria, VA , 1992, pp. 757–765.

[7]Hofmann-Wellenhof, B., Lichtenegger, H., and Collins, J., *GPS Theory and Practice*, Springer–Verlag, Vienna, 1992.

[8]Cohen, C. E., "Attitude Determination," *Global Positioning System: Theory and Applications*, Vol. 2, edited by B. W. Parkinson, J. J. Spilker, P. Axelrad, and P. Enge, Vol. 164, Progress in Astronautics and Aeronautics, AIAA, Washington, DC, 1996, pp. 519–538.

[9]Wertz, J. R. (ed.), *Spacecraft Attitude Determination and Control*, Kluwer Academic Publishers, Dordrecht, The Netherlands, 1978, Chap. 15.

[10]Cohen, C. E., "Attitude Determination Using GPS," Ph.D. Dissertation, Dept. of Aeronautics and Astronautics, Stanford Univ., Stanford, CA, Dec. 1992.

[11]Anon., *TANS Vector Specification and User's Manual*, Trimble Navigation Limited, Sunnyvale, CA, 1993.

[12]Axelrad, P., and Chesley, B. C., "Performance Testing of a GPS Based Attitude Determination System," *Proceedings of the AIAA Guidance, Navigation, and Control Conference* (Monterey, CA), AIAA, Washington, DC, 1993, pp. 809–819.

[13]Kay, S. M., *Modern Spectral Estimation Theory & Application*, Prentice–Hall, Englewood Cliffs, NJ, 1988, Chap. 7.